Nanoscale

ROYAL SOCIETY OF CHEMISTRY

PAPER

View Article Online
View Journal | View Issue

Check for updates

Cite this: *Nanoscale*, 2020, **12**, 17362

Rapid and sensitive quantification of cell-associated multi-walled carbon nanotubes†

Lukas Steinmetz, [a] Joel Bourquin, [a] Hana Barosova, [a] Laetitia Haeni, [a] Jessica Caldwell, [a] Ana Milosevic, [b] Christoph Geers, [a] Mathias Bonmarin, [c] Patricia Taladriz-Blanco, *[a] Barbara Rothen-Rutishauser [a] and Alke Petri-Fink *[a,d]

Received 28th April 2020,
Accepted 8th July 2020

DOI: 10.1039/d0nr03330h

rsc.li/nanoscale

Evaluating nanomaterial uptake and association by cells is relevant for *in vitro* studies related to safe-by-design approaches, nanomedicine or applications in photothermal therapy. However, standard analytical techniques are time-consuming, involve complex sample preparation or include labelling of the investigated sample system with *e.g.* fluorescent dyes. Here, we explore lock-in thermography to analyse and compare the association trends of epithelial cells, mesothelial cells, and macrophages exposed to gold nanoparticles and multi-walled carbon nanotubes over 24 h. The presence of nanomaterials in the cells was confirmed by dark field and transmission electron microscopy. The results obtained by lock-in thermography for gold nanoparticles were validated with inductively coupled plasma optical emission spectrometry; with data collected showing a good agreement between both techniques. Furthermore, we demonstrate the detection and quantification of carbon nanotube-cell association in a straightforward, non-destructive, and non-intrusive manner without the need to label the carbon nanotubes. Our results display the first approach in utilizing thermography to assess the carbon nanotube amount in cellular environments.

Open Access Article. Published on 13 August 2020. Downloaded on 2/6/2026 6:09:53 PM.
This article is licensed under a Creative Commons Attribution 3.0 Unported Licence.

1 Introduction

The investigation of fundamental interactions of nanoparticles (NPs) with biological systems is a prominent area of research with increasing patent applications, funding, and scientific publications.[1–3] The reasons for the rapid growth of research activities in this field include economic (*i.e.*, faster commercialization) or health-related (*i.e.*, understanding their potential risk and hazard) factors. Imaging techniques including electron microscopies, confocal laser scanning microscopy, or dark field microscopy are typically used to study NP-cell interactions. The choice of technique strongly depends on the studied NPs and the use of fluorescent dyes. For example, fluorescent labeling and staining of NPs and cells, respectively, allows for live cell imaging and thereby enables one to perform co-localization studies and real time observations of particle-cell interactions. However, it has been shown that the presence of surface-attached fluorescent dyes can strongly change NP-cell interactions.[4] Furthermore, these dyes are prone to quenching, leading to inaccurate fluorescent signals, *e.g.*, during the detection of gold NPs (AuNPs).[5] Quantitative data can be added in this context by using inductively coupled plasma spectroscopy (ICP), which involves the chemical digestion of organic matter (*i.e.*, cells, proteins, *etc.*) and dissolution of the AuNPs before quantifying the amount of gold in solution.[6,7]

When moving from model AuNPs to analytically more complex multi-walled CNTs (MWCNTs), which have become one of the most widely used carbon-based materials,[8,9] the study of their interaction with cells becomes more challenging. Although it is possible to image CNTs associated to cells with dark field and electron microscopy, their detection and quantification in biological samples is arguably more demanding than the previously described AuNPs due to the fact that (i) CNTs do not show plasmonic properties, (ii) their contrast is comparably low, (iii) their solubility and stability in aqueous solution is limited, and (iv) they are only indirectly quantifiable by ICP and rely on the presence of metal catalyst impurities (related to the synthesis process).[10,11] Other techniques, such as stereology, radio-labelled ^{14}C-CNTs or electrophoretic

[a]*Adolphe Merkle Institute, University of Fribourg, Chemin des Verdiers 4, 1700 Fribourg, Switzerland. E-mail: alke.fink@unifr.ch, patricia.taladrizblanco@unifr.ch*
[b]*Swiss Federal Laboratories for Materials Science and Technology (Empa), Lerchenfeldstrasse 5, 9014 St. Gallen, Switzerland*
[c]*School of Engineering, Zurich University of Applied Sciences, Technikumstrasse 9, 8400 Winterthur, Switzerland*
[d]*Chemistry Department, University of Fribourg, Chemin des Verdiers 4, 1700 Fribourg, Switzerland*

†Electronic supplementary information (ESI) available. See DOI: 10.1039/d0nr03330h

This journal is © The Royal Society of Chemistry 2020

Open Access Article. Published on 13 August 2020. Downloaded on 2/6/2026 6:09:53 PM.
This article is licensed under a Creative Commons Attribution 3.0 Unported Licence.

separation methods, which have been used for this purpose, involve tremendous workloads.[12,13] However, CNTs are efficient light absorbers and exhibit high thermal conductivities, which renders them suitable for photothermal applications,[14–19] and in turn opens up a door for thermography.

Lock-in thermography (LIT) is a heat-sensitive imaging technique which allows the visualization and characterization of plasmonic NPs in a sample due to their ability to generate heat in response to an external stimulus.[20,21] In a recent study, the applicability of LIT for plasmonic NPs has been demonstrated, highlighting how NP aggregation can be resolved by changing the excitation wavelength.[22] LIT is based on exposing the sample to a periodic amplitude-modulated stimulation, while continuously imaging with an infrared (IR) camera to monitor the sample surface temperature over time. Instead of monitoring the change in temperature over time, the amplitude of the temperature oscillations (*i.e.*, between on and off states of the external stimulus) is determined, thus enabling the selective filtering of background noise that is not originating from the stimulus.[23,24] By using a sensitive IR camera and averaging the signal over numerous cycles, LIT is able to measure temperature differences down to 0.001 K.[25]

In this study, we demonstrate the use of LIT to qualitatively assess the interaction of CNTs and AuNPs with cells. As a proof of concept, we studied the association of 14 nm and 42 nm AuNPs with different cell types, such as epithelial cells, mesothelial cells, and macrophages, over 24 h. The quantity of cell-associated NPs was estimated using the LIT technique and compared to quantitative data obtained by ICP-OES. Our results for these experiments show that LIT can reliably probe NP-cell interactions. We also studied the association of Mitsui-7 and Nanocyl MWCNTs to cells. We then established a calibration curve by exposing cells to known concentrations of CNTs in order to estimate the amount of CNTs associated to the different cell lines. To the best of our knowledge, it is the first time that a thermography technique is used to quantitatively assess the amount of CNTs associated to cells. We highlight that LIT is a straightforward and cost-effective technique, which can be used by researchers in the field of bionanotechnology to assess nanomaterial (NM)-cell association without dye-labelling or other laborious sample preparation. Furthermore, LIT can be used for the analysis of CNTs, enabling fast and sensitive detection and quantification of cell-associated CNTs.

2 Experimental section

2.1 Synthesis of polyvinylpyrrolidone-functionalized gold nanospheres (Au@PVP)

AuNPs were prepared by the Turkevich method.[26] Briefly, a 0.5 mM gold solution (99% tetrachloroauric acid, $HAuCl_4 \cdot 3H_2O$, Sigma-Aldrich, Switzerland) was boiled in the presence of 1.5 mM of sodium citrate (≥98%, $C_6H_5Na_3O_7 \cdot 2H_2O$, Sigma-Aldrich, Switzerland). The resulting citrate capped AuNPs with a core diameter of 14 nm were functionalized with polyvinylpyrrolidone (PVP 8000 g mol^{-1}, $(C_6H_9NO)_n$, Acros Organics, Switzerland), by mixing 0.47 mM of Au sols with a 2.65 mM PVP aqueous solution. 42 nm AuNPs were prepared by reduction of gold salt (0.25 mM) with hydroxylamine hydrochloride (0.2 M) in the presence of sodium citrate (0.5 mM) and as-prepared citrate capped 14 nm AuNPs (0.0125 mM). Particles were subsequently functionalized with PVP (1.1 mM) as described for 14 nm AuNPs.[27]

2.2 Preparation of Mitsui-7 and Nanocyl MWCNTs dispersions

Pre-weighed dry Mitsui-7 (kind gift of Prof. Vicki Stone, Heriot-Watt University, Edinburgh, UK; Mitsui & Co, Japan) and Nanocyl-7000 MWCNTs (Nanocyl SA, Belgium; JRCNM4000a, received from European Commission Joint Research Centre, Italy) powders were suspended in 0.05 mg mL^{-1} of bovine serum albumin (BSA, Sigma-Aldrich, Switzerland) ([MWCNTs] = 200 μg mL^{-1}). The suspension was then sonicated using a probe sonicator (Sonifier SFX550, Branson Ultrasonics Corp., USA) for 10 min at 21% amplitude under cooling. The suspension was stored at 4 °C and sonicated for 30 min in a water bath before use. The preparation of the MWCNTs was performed according to the NanoReg protocol, with the exception of the CNT concentration, which was adjusted (200 instead of 2560 μg mL^{-1}).[28]

2.3 Coating of cell culture plates

48-Well plates were coated with Fibronectin and Collagen I to optimize cell adhesion for all cell types. 600 μL of phosphate-buffered saline (PBS) solution supplemented with 0.1 mg mL^{-1} of BSA, 0.03 mg mL^{-1} Vitrogen 100 (Collagen I, bovine) and 0.01 mg mL^{-1} Fibronectin (BD Laboratories, Switzerland) were placed in each well and incubated for 3 h at 37 °C and 5% CO_2. Subsequently, the solution was removed, and the plates were stored at 4 °C until use. Plates were used within a month after coating.

2.4 Cell culture

Mouse macrophage cell line J774A.1 and human alveolar epithelial cell line A549 (both ATCC, Switzerland) were cultivated in Roswell Park Memorial Institute 1640 (RPMI, Gibco, Life Technologies Europe B.V., Switzerland) cell culture medium supplemented with fetal bovine serum (FBS, 10 vol%, PAA Laboratories, Chemie Brunschwig AG, Switzerland, Life Technologies Europe B.V., Switzerland), L-glutamine (1 vol%, Gibco, Life Technologies Europe B.V., Switzerland), penicillin (100 units per mL, Gibco, Life Technologies Europe B.V., Switzerland) and streptomycin (100 μg mL^{-1}, Gibco, Life Technologies Europe B.V., Switzerland), from now on referred to as complete RPMI (cRPMI).

Human mesothelial cell line MeT-5A (ATCC, USA) was cultured in medium-199 (Gibco, Life Technologies Europe B.V., Switzerland) supplemented with 10 vol% FBS, penicillin, streptomycin, 3.3 nM epidermal growth factor (EGF) (final concentration), 400 nM hydrocortisone (final concentration), 870 nM

Open Access Article. Published on 13 August 2020. Downloaded on 2/6/2026 6:09:53 PM.
This article is licensed under a Creative Commons Attribution 3.0 Unported Licence.

insulin (final concentration), 20 mM HEPES (final concentration), 0.3869 mg L^{-1} sterile filtered selenous acid (Sigma-Aldrich, Switzerland), and 1 : 1000 Trace Elements B (Corning™, ThermoFisher Scientific, Switzerland), from now on referred to as complete medium-199 (cM199).

The human bronchial epithelial cell line 16HBE14o-, a generous gift from Dr D. Gruenert (Cardiovascular Research Institute, University of California, San Francisco, USA), was cultured in minimum essential medium (MEM, Gibco, Life Technologies Europe B.V., Switzerland) supplemented with 10 vol% FBS, penicillin and streptomycin, from now on referred to as complete MEM (cMEM).

Cells were grown in cell culture flasks (TPP Techno Plastic Products AG, Switzerland) and kept at 37 °C, 5% CO_2 and 95% humidity. At around 80% of cell confluence, the growth medium was exchanged and the cells were either scraped (J774A.1) or detached (A549, MeT-5A and 16HBE14o-) with a mixture of trypsin and EDTA (T/E, 0.25%, sterile-filtered, Gibco, Life Technologies Europe B.V., Switzerland). For J774A.1 and A549 cells, 10 vol% of the total cell suspension was then added to a new flask and supplemented with the corresponding fresh medium. In the case of MeT-5A 15 vol% and in the case of 16HBE14o- 25 vol% of the cell suspension was transferred to the new flask. The remaining cell suspension was used to perform the experiments and its cell concentration was determined by using the trypan blue assay and an automated cell counter (EVE, NanoEnTek Inc., South Korea). For this, the cell suspension was mixed at a 1 : 1 volume ratio with trypan blue (Sigma-Aldrich, USA) and pipetted into a cell counting slide.

The exposure experiments were carried out by seeding 75.000 cells (A549, MeT-5A and J774A.1) or 125.000 cells (16HBE14o-) per well in 1 mL of corresponding cell culture medium (cCCM) in the above described pre-coated 48-well plates and left growing for 48 h. Cell confluency was assessed with bright field imaging and ImageJ v1.52b (NIH, USA). The coverage percentage was calculated using 3 individual images for every condition. Afterwards, the cells were exposed to either 10 μg mL^{-1} of MWCNTs (Mitsui-7 and Nanocyl) or 20 or 50 μg mL^{-1} of AuNPs (14 nm or 42 nm) previously dispersed in the corresponding cCCM. The samples were incubated for 0, 2, 7, 16, 20, and 24 h, washed 3 times with PBS to remove non-associated NPs, and subsequently dried in the desiccator overnight. Samples were prepared in triplicate.

2.5 Lock-in thermography (LIT)

The NM-cell association was determined by recording the NM heat generation using LIT. As previously reported, a custom-made experimental setup, consisting of a homogeneous LED-based light source which emits excitation light at various wavelengths; 400 nm, 525 nm and 730 nm (AN178 2 61 LED module, ADOM); an infrared camera (Onca-MWIR-InSb-320, XenICs, Belgium) mounted on a standard microscope stand (Leica Microsystems, Germany) and a personal computer as a processing unit was used to carry out the measurements.[21,22,24]

Homogeneous spatial illumination of the sample was ensured by placing a light homogenizing glass rod (N-BK7, Edmond Optics, USA) between the LED panel and the sample. All samples were loaded into custom-made, spherical and light transparent sample holders.

The camera InSb array (320 × 256 pixels) operating in the mid-IR range (3 to 5 μm) is capable of capturing full frame images at a rate up to 200 Hz. A custom-made LabVIEW-based software was employed to perform the data processing in real time.[24] The software demodulates the acquired infrared images according to the digital lock-in principle to compute amplitude maps (in Kelvin).[23]

The resulting amplitude images were evaluated by using ImageJ v1.52b and Origin 2016 (OriginLab, USA) to extract the mean signal over the sample holder area and calculate the standard deviation.

All measurements were performed using a stimulation frequency of 1 Hz and an applied current of 150 mA for 400 nm and of 200 mA for 525 nm and 730 nm LEDs, resulting in power densities of 58.7 mW cm^{-2}, 74.2 mW cm^{-2} and 114.4 mW cm^{-2}, respectively. The duration of a single measurement was set to 60 s (*i.e.*, 60 cycles), kept constant for every sample, and repeated five times consecutively.

2.6 UV-Vis spectroscopy (UV-Vis)

UV-Vis spectra of AuNPs and MWCNTs were recorded at room temperature to observe the evolution of the NMs in cCCM with a V-670 spectrophotometer (Jasco, USA) using 10 mm path length quartz suprasil cuvettes (Hellma Analytics, Germany) and 8.5 mm path length micro UV-cuvettes (Brand, Germany). For UV-Vis measurements over 24 h spectra were taken every hour.

2.7 Inductively coupled plasma optical emission spectrometry (ICP-OES)

For the analysis of cell-associated AuNP content, ICP-OES (PerkinElmer Avio-200, USA, axial-viewing, λ = 267.595 nm) measurements using a radio frequency power of 1500 W, gas flow rates of 8 L min^{-1} (Ar, plasma) and 0.2 L min^{-1} (N2, auxiliary), pump 0.7 L min^{-1} (nebulizer), and 1 mL min^{-1} sample flow rate (equilibration delay of 15 s) were performed. Before the analysis, all samples were digested to remove the organic matter from the cells and dissolve the AuNPs. Briefly, samples were frozen at −80 °C and subsequently thawed in steps; first to −20 °C, then 4 °C and finally room temperature with 2 h in between each temperature step. 300 μL of a 2 : 1 mixture of HNO_3 and H_2O_2 were added to every sample and left for pre-digestion for 3 h. Subsequently, all samples were sonicated at 50 °C for 15 min. Finally, 400 μL of HCl was added to each well and left overnight at room temperature for digestion. The next day, the solutions were transferred to Falcon tubes and diluted to 5 mL. The same procedure was performed for 10 gold standards (Sigma-Aldrich, Switzerland).

This journal is © The Royal Society of Chemistry 2020

Open Access Article. Published on 13 August 2020. Downloaded on 2/6/2026 6:09:53 PM.
This article is licensed under a Creative Commons Attribution 3.0 Unported Licence.

2.8 Transmission electron microscopy (TEM)

A Tecnai Spirit transmission electron microscope (FEI, USA) operating at 120 kV was used to visualize and confirm the presence of NMs in and on cells. 300.000 cells (A549) per well were seeded on a 6-well plate and incubated for 48 h. After incubation the cells were exposed to 50 μg mL^{-1} of AuNPs or 10 μg mL^{-1} of MWCNTs for 24 h, further washed and fixed using 4 vol% paraformaldehyde (PFA) and 2.5 vol% glutaraldehyde (both Sigma-Aldrich, Switzerland) in PBS. The samples were then stained using Osmium tetroxide (OsO_4), embedded in resin and sectioned with an ultramicrotome (performed by the Microscopy Imaging Center (MIC), University of Bern, Switzerland). Finally, the sections were mounted on a copper carbonated TEM grid for analysis. Images were acquired with a Veleta CCD camera (Olympus, Japan) and treated with the ImageJ software (v1.52b).

2.9 Fluorescence-enhanced dark field microscopy (DF)

Fluorescence-enhanced dark field imaging was used to visualize the association of AuNPs and MWCNTs with cells. 1 mL per well of cell suspensions (40.000 cells per mL) was seeded in a 4-well microscopy slide. After overnight attachment, the cells were exposed to 20 μg mL^{-1} of AuNPs or 10 μg mL^{-1} of MWCNTs and incubated for 24 h. Then, the cells were washed 3 times with PBS and fixed with 4 vol% PFA in PBS for 10 min at room temperature. The cells were washed with washing buffer (PBS supplemented with 0.1 vol% BSA and 0.001 vol% sodium azide) for 5 min, permeabilized in 0.2 vol% Triton X-100 in PBS for 10 min at room temperature, and washed three times with washing buffer for approximately 2 min per wash. Then the cells were stained using DAPI (100 μg mL^{-1}) and Phalloidin Rhodamine (1 : 100) in PBS supplemented with 0.1 vol% Triton X-100 and 1 vol% BSA for 1.5 h at room temperature in the dark. The staining solution was discarded and the cells were washed 5 times with PBS for 5 min each. After removing the PBS, a drop of Glycergel mounting medium was added onto the cells and then covered with a glass cover slip.

The cells were then imaged using a CytoViva hyperspectral microscope (CytoViva, Inc., USA) equipped with a Dolan-Jenner DC-950 light source, UPL Fluorite 100x objective and SPECIM V10E imaging spectrograph with a PCO pixel detector (HSI) and 3D (EXi Blue) fluorescence/dark field detector.

2.10 Dynamic light scattering (DLS) and zeta potential

The hydrodynamic diameter (D_h) and the zeta-potential of the PVP-functionalized AuNPs were analysed with a 90Plus Particle Size Analyzer (Brookhaven, USA). To assess the stability of AuNPs in cCCM depolarized DLS (DDLS) measurements were performed, using a commercial goniometer instrument (3D LS Spectrometer, LS Instruments AG, Switzerland). Samples were measured at 37 °C over 24 h. The effective surface charge of the NPs was evaluated using phase-amplitude light scattering (ZetaPALS, Brookhaven, USA) in water. To estimate the mean and the standard deviation, ten DLS and zeta potential measurements were recorded for each sample.

2.11 Calibration of quantification of Nanocyl MWCNTs

1 mL per well of an A549 cell suspension (75.000 cells per mL) was seeded into pre-coated 48-well plates. After 48 h of cell growth, the cells were washed with PBS and exposed to a known amount of Nanocyl MWCNTs (0; 0.5; 1; 1.5; 2; 2.5; 3; 4; 6; 8; 10 and 12 μg) in 300 μL of Milli-Q water. Immediately after exposure, samples were completely dried in an oven at 37 °C.

2.12 Limit of detection (LOD) and quantification (LOQ)

The LOD and the LOQ in all figures were obtained by 95% confidence bands after Hubaux and Vos.[29]

3 Results and discussion

Prior to the NP-cell association studies, the stability of PVP-functionalized AuNPs and BSA-coated MWCNTs in different complete cell culture media (cCCM) was investigated by UV-Vis spectroscopy (Fig. S1†). Overall, AuNPs remained stable in all media with the exception of 14 nm AuNPs in cM199, which can potentially be explained by the presence of selenous acid in the medium (Fig. S1A–F†).[30] These findings were also confirmed by DDLS measurements (Table S1†). Rapid sedimentation of Mitsui-7 MWCNTs in cCCM was observed within 24 h (Fig. S1G–I†), while Nanocyl MWCNTs remained stable in the dispersion (Fig. S1J–L†). Table 1 summarizes the physicochemical characteristics of the NMs used in this study.

In order to test the versatility of the LIT technique to investigate NP-cell association, different cell lines were used, *i.e.*, human epithelial type-II cells A549, bronchial epithelial cells 16HBE14o-, immortalized mesothelial cells MeT-5A, and J774A.1 murine macrophages. The first three cell types form confluent epithelial and mesothelial cell monolayers, allowing for measurements to determine the produced heat per surface area of a single cellular layer. J774A.1 was included due to the

Table 1 Summary of relevant material parameters of the investigated PVP-functionalized AuNPs and MWCNTs recorded in water. It was not possible to determine the hydrodynamic diameter (D_h) and zeta potential of MWCNTs, as these materials are highly polydisperse and exhibit large aspect ratios

	AuNPs		MWCNTs	
	14 nm	42 nm	Mitsui-7	Nanocyl
Diameter (TEM) [nm]	14 ± 1	42 ± 4	—	—
Length [nm][a]	—	—	5660 ± 4700	850 ± 457
Width [nm][a]	—	—	60 ± 19	11 ± 5
Aspect ratio (length/width)	—	—	94	77
D_h (DLS) [nm]	21 ± 2	51 ± 3	—	—
Zeta potential [mV]	−9.8 ± 4	−12.0 ± 10	—	—
Max. absorbance [nm]	519	525	<300	<300

[a] The dimensions of the CNTs were taken from Chortarea *et al.* and Poulsen *et al.*[31,32]

Open Access Article. Published on 13 August 2020. Downloaded on 2/6/2026 6:09:53 PM.
This article is licensed under a Creative Commons Attribution 3.0 Unported Licence.

fact that they are professional-phagocytic cells that efficiently take up diverse NPs. As these cells do not form confluent monolayers, a heat signal which was not evenly distributed was expected.

The association of cell-exposed NMs, *i.e.*, attached to the cell membrane and/or internalized, was first assessed by using fluorescence-enhanced dark field microscopy (DF) and transmission electron microscopy (TEM) (Fig. 1 and 2) after 24 h of exposure. As shown in Fig. 1a, the overlay of DF images and fluorescence micrographs confirms that both 14 nm and 42 nm AuNPs show a high degree of association for all tested cell types (F-Actin stained). As expected, due to their phagocytic nature, J774A.1 macrophages seem to incorporate more NPs (independent of their size) compared to the other cell types.[33] Furthermore, by using TEM, the subcellular location of the AuNPs was investigated in A549 cells. Both the 14 nm (Fig. 1b) and the 42 nm (Fig. 1c) AuNPs can be observed intracellularly grouped; presumably in endolysosomal vesicles.[34,35]

As with AuNPs, the association of MWCNTs with the cells was confirmed. Mitsui-7 MWCNTs were clearly detectable with both techniques, whereas it was not possible to image Nanocyl MWCNTs with TEM (Fig. 2b) due to their smaller size and low contrast. DF indicated that Nanocyl are densely packed in cellular vesicles, which can be explained by their tangled shape compared to Mitsui-7, and thus a localization in the *endo*-lysosomal system is expected (Fig. 2a).[36]

3.1 Cell associated AuNPs

Cells were exposed to 20 or 50 μg mL^{-1} of AuNPs for up to 24 h to investigate their association with cells over time. After 2, 7, 16, 20 or 24 h, the cells were washed with phosphate-buffered saline (PBS) to remove the loosely attached and non-attached NPs. Once washed, the samples were completely dried in a desiccator to avoid artifacts that could influence their heat generation caused by the cCCM. After drying, the heat production from AuNPs was evaluated using LIT. Additionally, it should be stated that LIT measurements cannot distinguish between membrane-attached and internalized NPs, as LIT records 2D amplitude images from 3D samples. Therefore, only association trends can be investigated.

A control measurement with untreated cells was performed and the LIT NP-cell association trends were compared to ICP-OES data. The investigated AuNPs with diameters of 14 nm and 42 nm most efficiently absorb light around a wavelength of 520 nm in their dispersed state. However, it has been shown that NPs attached to the cells' surface are often aggregated or clustered, which strongly alters their light absorbance and scattering behaviour (Fig. S2†).[37] Therefore, it is very likely that in the presence of cells both single NPs and aggregates contribute to the heat generation upon light irradiation. In consequence, two different wavelengths (525 nm and 730 nm) were used to irradiate the cell-exposed AuNPs to account for single and aggregated AuNPs.[38] It is important to note that aggregated AuNPs absorb light over a broad wavelength range and therefore also contribute to signal obtained from excitation at 525 nm (Fig. S2,† red spectra), while single NPs do not generate any detectable heat when excited at 730 nm (Fig. S2,† black spectra).

Fig. 3 shows the amplitude signal (*i.e.*, the generated heat) obtained by LIT and ICP-OES data of 14 and 42 nm AuNPs at two different concentrations (*i.e.* 20 and 50 μg mL^{-1}) for fully confluent cells (*i.e.*, A549, 16HBE14o-, and MeT-5A cells). The measured heat signals and the NP concentrations obtained by ICP-OES show comparable trends over 24 h. Both methods highlight that the MeT-5A (Fig. 3, blue triangles) cells associate more NPs, which was demonstrated for both NP sizes and exposure concentrations. Interestingly, saturation is reached for the 14 nm AuNPs only at 50 μg mL^{-1} at roughly 16 h, whereas no plateau is reached at the lower concentration of 20 μg mL^{-1}. In contrast, 42 nm AuNPs reach a plateau at approximately 7 h independently of NP concentration.

No distinct difference is observed between A549 (Fig. 3, black squares) and 16HBE14o- (Fig. 3, red dots) cells, although A549 generally seem to have a slightly increased NP association, with the only exception being the ICP-OES results of 20 μg mL^{-1} in the case of the 42 nm NPs. Both cell lines do not show saturation in case of the smaller 14 nm NPs for either concentration. When using 42 nm AuNPs the association reaches a plateau similar to the MeT-5A cells, but at a lower level.

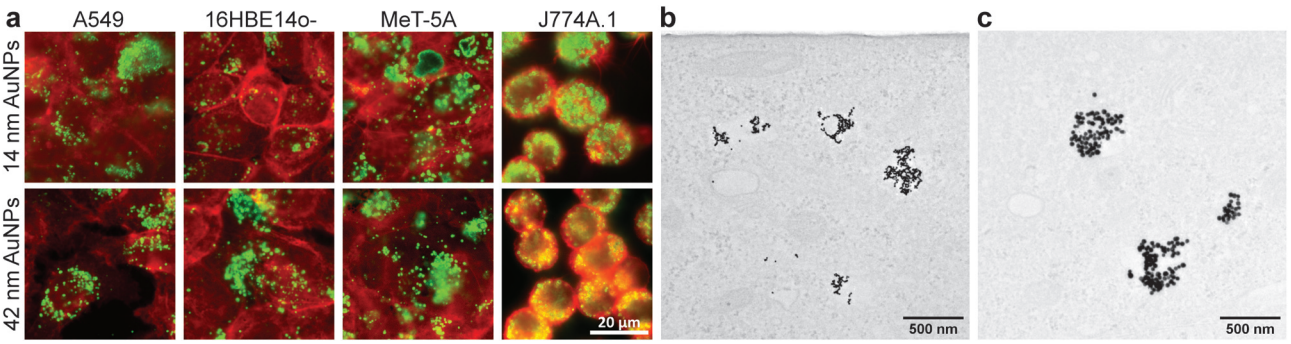

Fig. 1 Visualization of AuNP-cell association for 14 nm and 42 nm NPs to confirm their presence inside of and on the surface of the four investigated cell types. Overlay of DF microscopy of AuNPs (green) and fluorescence microscopy for various cell types (red) (a). TEM micrographs of 14 nm (b) and 42 nm (c) AuNPs in A549 cells.

 This journal is © The Royal Society of Chemistry 2020

Open Access Article. Published on 13 August 2020. Downloaded on 2/6/2026 6:09:53 PM.
This article is licensed under a Creative Commons Attribution 3.0 Unported Licence.

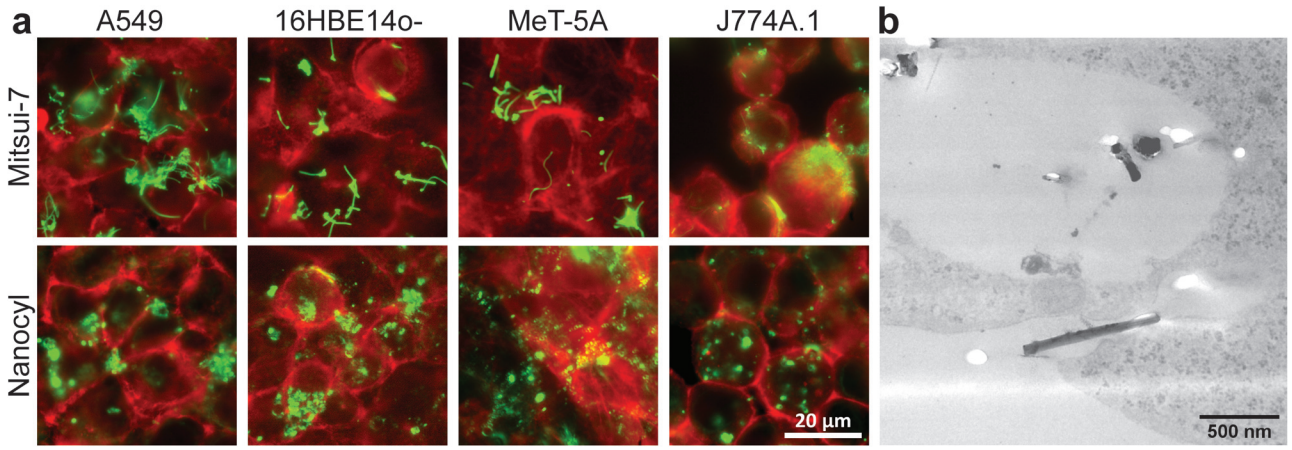

Fig. 2 Visualization of MWCNT-cell association for Mitsui-7 and Nanocyl MWCNTs to confirm the presence of CNTs in and on the surface of the four investigated cell types after exposure for 24 h. Overlay of DF microscopy of MWCNTs (green) and fluorescence microscopy for various cell types (red) (a). TEM micrograph of Mitsui-7 in A549 cells (b).

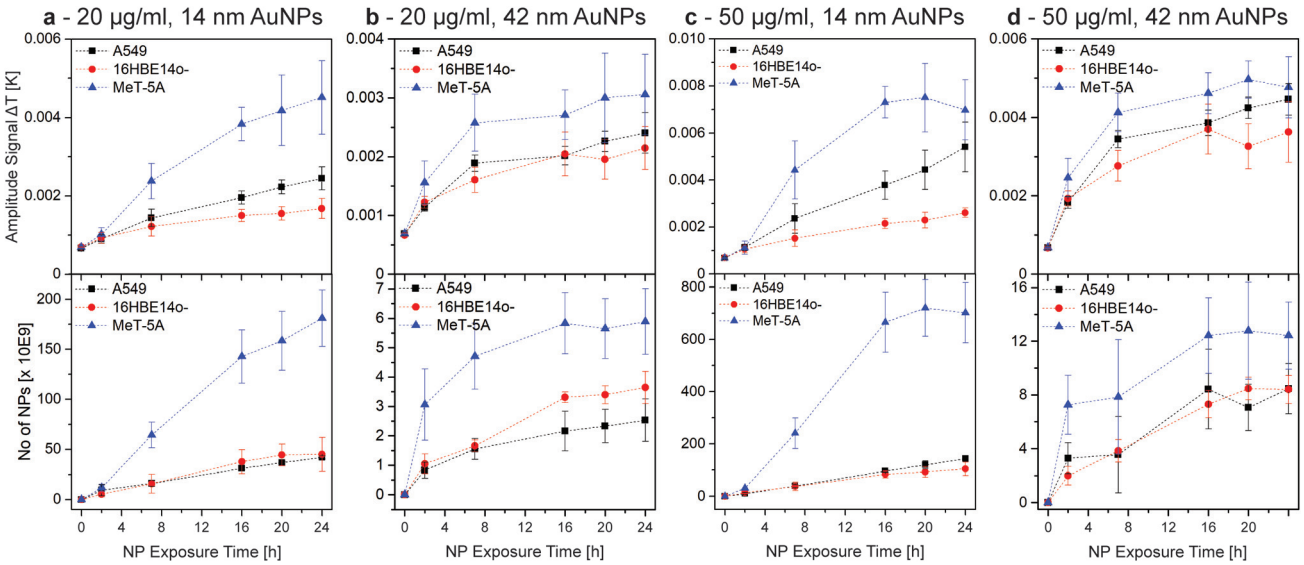

Fig. 3 AuNP-cell association trends over 24 h, obtained by LIT (top row, 525 nm excitation wavelength) and ICP-OES (bottom row). The association trends of A549, 16HBE14o-, and MeT-5A cells exposed to 20 and 50 µg mL^{-1} of 14 nm (a and c) and 42 nm AuNPs (b and d) were investigated. Hence, it was possible to determine that, independent of the NP size and concentration, the AuNP association is higher for MeT-5A. The plateau reached under some conditions indicated a NP-cell association saturation. This figure is re-printed as Fig. S6 with identical *y*-axes in the ESI† to facilitate the comparison of AuNP sizes and concentrations for the reader.

As the LIT amplitude signal is related to the available cell surface area and J774A.1 cells do not form a confluent layer, LIT measurements were adjusted to compensate for the fact that the cells do not cover the whole well surface. Using phase contrast imaging, the surface of J774A.1 covering the well was determined and used to scale the generated heat to a hypothetically 100% confluent cell population to enable the comparison with the other cell lines. The comparison between the results of the mesothelial (MeT-5A) and epithelial (A549 and 16HBE14o-) cells to the macrophages (J774A.1) (Fig. S3†) highlights the influence of the cell type in terms of NP association. Furthermore, results show that J774A.1 associate significantly more AuNPs than the epithelial cells, a behaviour similar to the mesothelial cells, while no plateau is reached for any of the conditions tested (Fig. 3 and S3†). These results demonstrate the efficiency of macrophages in terms of NP clearance from their surroundings.[33] However, direct comparison between the epithelial and mesothelial cells and the macrophages is difficult due to the difference in surface area coverage (*i.e.*, formation of cell monolayers at different levels of confluence), which strongly alters the number of associated NPs.

The observed differences between the NPs (sizes and concentrations) and cells can be explained by many factors. It has been shown that NP size, shape, degree of polydispersity, as

Open Access Article. Published on 13 August 2020. Downloaded on 2/6/2026 6:09:53 PM.
This article is licensed under a Creative Commons Attribution 3.0 Unported Licence.

well as protein-corona formation can strongly influence NP-cell interactions.[39–43] In this study, the use of different cell culture media (cRPMI, cMEM or cM199) could influence the NP-protein interaction, or enhance the sedimentation/diffusion profile of the NPs; consequently leading to altered cell-association.[44–46] Furthermore, depending on the origin of the cells, cell surface receptor density is different, which might impact NP-cell association and ultimately NP uptake.[47] The latter supports the similar NP-cell association for A549 and 16HBE14o-, both human lung epithelial cells. Moreover, NPs can be internalized by various endocytic mechanisms (*e.g.*, caveolin-mediated and clathrin-mediated endocytosis). Preference for one uptake mechanism is dependent upon the NP size, which could explain the observed differences in uptake and association of the various NPs.[48,49]

For the AuNPs, no significant change in association for both LIT excitation wavelengths, 525 nm and 730 nm, was observed, indicating that NPs are either aggregated, or dispersed and aggregated, as all NPs show similar association characteristics (Fig. 4). These findings are valid for both exposure concentrations and both NP sizes. Additionally, the limit of detection (LOD) and quantification (LOQ) for an excitation wavelength of 525 nm was determined using the Hubaux and Vos approach.[29] A LOD of 11.8 μg mL^{-1} and a LOQ of 21.7 μg mL^{-1} was obtained for 14 nm AuNPs. For the 42 nm AuNPs, 5.9 μg mL^{-1} and 11.8 μg mL^{-1} were found for LOD and LOQ, respectively. In general, LIT exhibits a good precision and accuracy, with deviations from the mean value between 5–10%. However, LIT usually has a lower sensitivity when compared to *e.g.* confocal LSM or flow cytometry.

3.2 Cell associated CNTs

The different cell lines were exposed to 10 μg mL^{-1} of Mitsui-7 and Nanocyl over 24 h, while bearing in mind that both CNTs strongly vary in their size and stiffness (Table 1). Compared to Nanocyl, Mitsui-7 have a higher aspect ratio (94 *vs.* 77), are stiffer, and can pierce cell membranes (Fig. S4†).[50,51] Lower exposure concentrations for CNTs in comparison to AuNPs were applied, as a significant increase in cytotoxicity for increasing CNT concentration has been reported.[31] Samples were measured using LIT centred at a wavelength of 400 nm to excite the MWCNTs due to their increasing light absorbance in the lower wavelength range (Fig. S1†).

Results show that the amplitude signal increases in the first hours, indicating that more CNTs are associated with cells over time, independently of the cell line or CNT type (Fig. 5). After 16 h, the heat generation reaches a saturation. As observed for the AuNPs, this behaviour cannot be reproduced

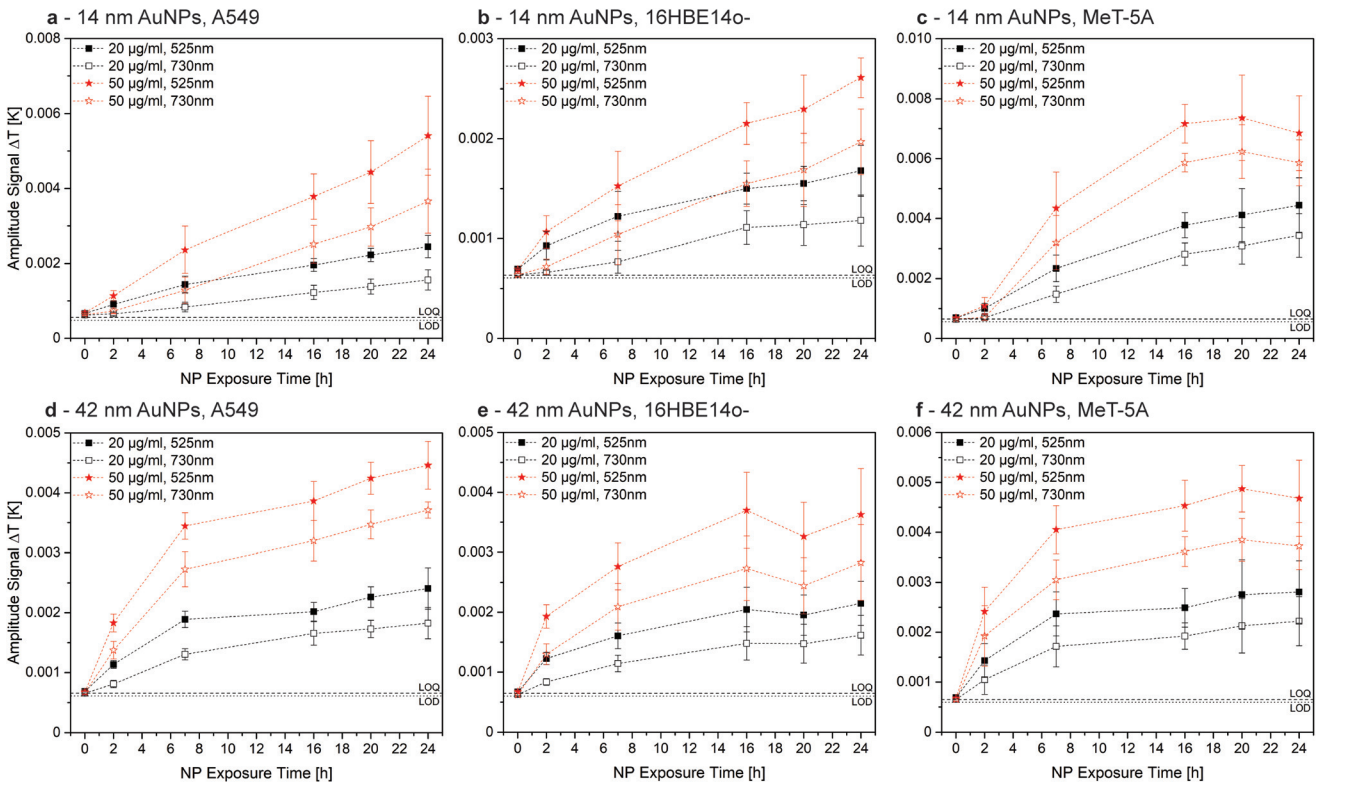

Fig. 4 Comparison of LIT measurements for cell-associated 14 nm (a–c) and 42 nm (d–f) AuNPs at an excitation wavelength of 525 nm (closed symbols) and 730 nm (open symbols). The generation of heat at an excitation wavelength of 730 nm is a clear indication for NP aggregation. However, association trends for 20 μg mL^{-1} (black symbols) and 50 μg mL^{-1} (red symbols) evolve in an almost identical manner over time. Therefore, either all AuNPs aggregate due to the association or single NPs and aggregates associate to a similar extent. This figure is re-printed as Fig. S7 with identical *y*-axes in the ESI† to facilitate the comparison of AuNP sizes and concentrations for the reader.

This journal is © The Royal Society of Chemistry 2020

Open Access Article. Published on 13 August 2020. Downloaded on 2/6/2026 6:09:53 PM.
This article is licensed under a Creative Commons Attribution 3.0 Unported Licence.

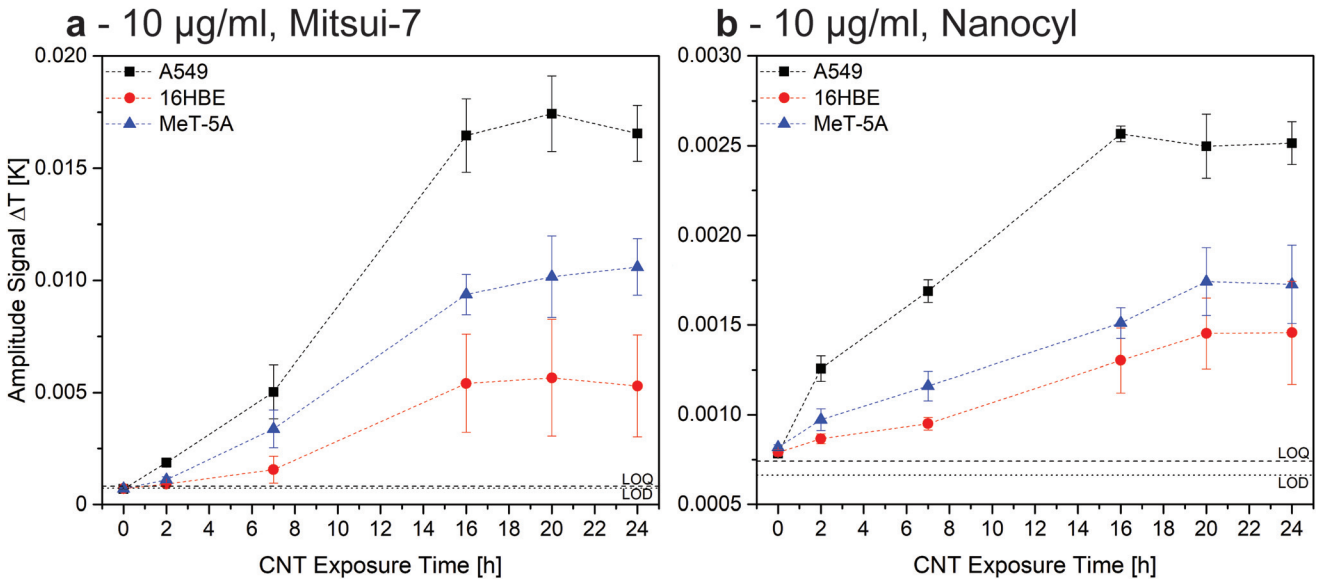

Fig. 5 MWCNT-cell association over 24 h, obtained by LIT. The association of A549, 16HBE14o-, and MeT-5A cells exposed to 10 µg mL^{-1} of Mitsui-7 (a) and Nanocyl (b) MWCNTs were analysed. Mitsui-7, despite their large size and poor uptake behaviour, generate significantly more heat than Nanocyl MWCNTs.

for J774A.1 cells (Fig. S5†) and the degree of the association depends on the cell type (Fig. 5 and Fig. S5†). Nonetheless, trends indicate that at the same exposure time, cells have comparably associated more Mitsui-7 than Nanocyl. This result might be explained by the higher dose of Mitsui-7 received by the cells after 24 h, caused by their faster sedimentation, which is related to the higher aspect ratio and higher stiffness in comparison to Nanocyl,[52,53] as has recently been reported by Septiadi *et al.*[51]

Fig. 5 shows that A549 cells associate more CNTs overall than MeT-5A and 16HBE14o- cells, independent of the MWCNT type. When comparing A549 and J774A.1 over 24 h, results show that the association of Mitsui-7 is higher for A549 than for J774A.1 (Fig. S5†). This observation is contradictory to the phagocytic nature of J774A.1 cells. However, this result is supported by the fact that cells hardly uptake Mitsui-7 MWCNTs due to their dimensions; instead, they pierce through the cellular membrane, or simply attach to it.[50] The

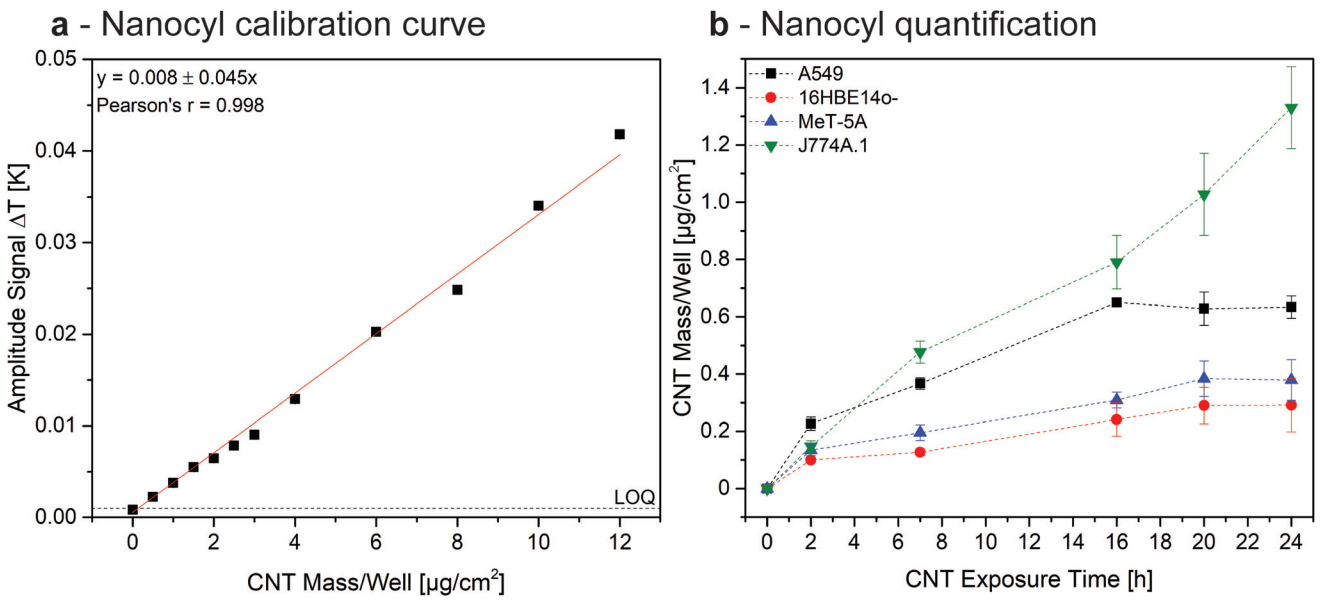

Fig. 6 Quantification of Nanocyl MWCNT content associated to the investigated cell types. Calibration curve, established with a known concentration of non-associated amounts of CNTs (a). CNT mass per well in different cell types, as determined by using the calibration curve (b).

Open Access Article. Published on 13 August 2020. Downloaded on 2/6/2026 6:09:53 PM.
This article is licensed under a Creative Commons Attribution 3.0 Unported Licence.

difference in confluency between J774A.1 and the three other cell lines can also help to explain this observation. Since J774A.1 covers only about 70% of the surface area, it is proposed that Mitsui-7 CNTs also attach to the free surface area in the system and are subsequently removed from the system by washing. In contrast, for the cells forming confluent layers, no free surface area is available and, therefore, it is assumed that the extent of non-associated CNTs is lower. As mentioned above, in the case of Nanocyl, the amplitude signal does not reach a plateau, which might indicate that Nanocyl is continuously taken up by the macrophages.

Since ICP cannot easily be performed to quantify the investigated MWCNTs associated to cells, as a proof of concept we established a calibration curve by recording the heat generated from samples containing a known amount of Nanocyl associated with A549. To do so, we chose Nanocyl over Mitsui-7 due to their enhanced dispersibility in water, but the quantification could in principle be performed for both of the investigated MWCNT types. Cells were grown as explained above and exposed to a defined amount of Nanocyl. As shown in Fig. 6a, LIT showed an accurate linear relationship (Pearson's r = 0.998) in the tested concentration range.

Extrapolating the data obtained in the Nanocyl exposure experiments (Fig. 5 and S5†), results show that the amount of CNTs associated to A549, 16HBE14o-, and MeT-5A cells increases linearly until reaching a maximum after 16 h of exposure, corresponding to a dose of 0.6 μg, 0.2 μg, and 0.25 μg, respectively (Fig. 6b). Since the initial total exposition dose was 5 μg, these values relate to 12%, 4%, and 5%, respectively. In contrast, the association of Nanocyl to J774A.1 experiences a continuous increase after 16 h, reaching an amount of 1.3 μg (26% of the total dose) of CNTs after 24 h. These results are in a comparable range with previously reported doses,[51] indicating LIT is a reliable tool for the quantification of cell-associated MWCNTs. However, the marginal amount of published papers focusing on quantifying MWCNT-cell association to date highlights the need for appropriate analytical methods within the field. The results reported in this paper show that LIT has the potential to be a powerful tool for use in such experiments.

4 Conclusion

In this study, we used LIT to investigate the collective heating effects of cell-associated nano-heaters. Relying on the thermoplasmonic behaviour of AuNPs and the ability of MWCNTs to generate heat, we were able to detect and characterize NM-cell association.

Two different sizes, 14 nm and 42 nm, and concentrations, 20 and 50 μg mL^{-1}, of PVP-functionalized AuNPs, as well as two different types of MWCNTs, Mitsui-7 and Nanocyl, were analysed. We exposed these NM systems to various cell lines, *i.e.*, epithelial cells, mesothelial cells, and macrophages. The degree of NM-cell association was determined at several time points over 24 h, which allowed us to draw conclusions about NM association trends in a precise and time-efficient way. Macrophages exhibited high association rates, however, comparing them to the epithelial and mesothelial cells has proven to be non-trivial due to their phagocytic nature and round single-cell morphology. In addition, we were also able to highlight the saturation point of NM-cell association. While macrophages seemed to constantly uptake NMs over 24 h, with the only exception being Mitsui-7 MWCNTs, which are likely too large and stiff to be uptaken by phagocytosis, epithelial and mesothelial cells exhibited varying saturation timepoints depending on the exposed NM size and concentration. For both investigated MWCNT types a plateau was observed after around 16 h, whereas diverse saturations were observed for AuNPs.

ICP-OES was used to validate the association trends of AuNPs with the different cells, confirming that LIT is a reliable tool for the analysis of NP-cell association. Due to the inherent heating properties of MWCNTs, LIT enables the quantification of Nanocyl associated with cells, which was demonstrated by using a calibration curve obtained by plotting the heat generated from samples where cells were exposed to a known concentration of Nanocyl.

Within this study, we exhibit that LIT is suitable to screen a large number of samples in a time-efficient manner without any complex sample preparation and *via* non-intrusive and non-destructive means, thus allowing the comparison of association trends. Especially for the detection and quantification of CNTs in cellular environments, we demonstrate in this work that LIT is a powerful tool, as the CNTs do not have to be modified or labelled, *e.g.*, with a fluorescent dye, before analysis. It is important to note that LIT is a complementary technique, which will not substitute established methods, such as TEM or ICP, but is a valuable asset for the nanotechnology community. For the future, the possibility to quantify complex NMs by LIT should be investigated in detail, due to its status as a time- and cost-effective analytical approach.

Author contributions

L.S., J.B., C.G., P.T.-B., B.R.-R. and A.P.-F. designed all experiments. L.S. synthesised the nanoparticles. J.B and L.H. performed the biological experiments. H.B. prepared the CNT dispersions. L.S. carried out the LIT measurements. All authors discussed the results and commented on the manuscript. L.S. and J.B. have contributed equally.

Conflicts of interest

For reasons of transparency we declare that 2 authors (CG and MB) have recently started a company, which specializes in lock-in thermal imaging instruments.

 This journal is © The Royal Society of Chemistry 2020

Open Access Article. Published on 13 August 2020. Downloaded on 2/6/2026 6:09:53 PM.
This article is licensed under a Creative Commons Attribution 3.0 Unported Licence.

Acknowledgements

This work was supported by the Swiss National Science Foundation (Grant No. 200021_184635 and 310030_159847/1), the University of Fribourg, and the Adolphe Merkle Foundation. Parts of this work were supported by the National Center of Competence in Research Bio-Inspired Materials. The authors would like to thank Nanolockin GmbH for the appropriation of their Calorsito prototype and Dr Miguel Spuch-Calvar for graphical support. We also want to thank Dr Sandor Balog for data treatment of the DDLS measurements, the Microscopy Imaging Center (MIC) of the University of Bern, Switzerland and Beat Haenni for the preparation of the TEM samples.

References

1 J. G. Teeguarden, P. M. Hinderliter, G. Orr, B. D. Thrall and J. G. Pounds, *Toxicol. Sci.*, 2007, **95**, 300–312.
2 A. P. Blum, J. K. Kammeyer, A. M. Rush, C. E. Callmann, M. E. Hahn and N. C. Gianneschi, *J. Am. Chem. Soc.*, 2015, **137**, 2140–2154.
3 D. Septiadi, F. Crippa, T. L. Moore, B. Rothen-Rutishauser and A. Petri-Fink, *Adv. Mater.*, 2018, **30**, 1–30.
4 L. Rodriguez-Lorenzo, K. Fytianos, F. Blank, C. Von Garnier, B. Rothen-Rutishauser and A. Petri-Fink, *Small*, 2014, **10**, 1341–1350.
5 A. M. Milosevic, L. Rodriguez-Lorenzo, S. Balog, C. A. Monnier, A. Petri-Fink and B. Rothen-Rutishauser, *Angew. Chem., Int. Ed.*, 2017, **56**, 13382–13386.
6 Y. N. Zhang, W. Poon, A. J. Tavares, I. D. McGilvray and W. C. W. Chan, *J. Controlled Release*, 2016, **240**, 332–348.
7 S. C. Wilschefski and M. R. Baxter, *Clin. Biochem. Rev.*, 2019, **40**, 115–133.
8 C. Cha, S. R. Shin, N. Annabi, M. R. Dokmeci and A. Khademhosseini, *ACS Nano*, 2013, **7**, 2891–2897.
9 M. F. L. De Volder, S. H. Tawfick, R. H. Baughman and A. J. Hart, *Science*, 2013, **339**, 535–539.
10 E. J. Petersen, D. X. Flores-Cervantes, T. D. Bucheli, L. C. C. Elliott, J. A. Fagan, A. Gogos, S. Hanna, R. Kägi, E. Mansfield, A. R. M. Bustos, D. L. Plata, V. Reipa, P. Westerhoff and M. R. Winchester, *Environ. Sci. Technol.*, 2016, **50**, 4587–4605.
11 C. Cheng, K. H. Müller, K. K. K. Koziol, J. N. Skepper, P. A. Midgley, M. E. Welland and A. E. Porter, *Biomaterials*, 2009, **30**, 4152–4160.
12 S. Rhiem, M. J. Riding, W. Baumgartner, F. L. Martin, K. T. Semple, K. C. Jones, A. Schäffer and H. M. Maes, *Environ. Pollut.*, 2015, **196**, 431–439.
13 T. Dos Santos, J. Varela, I. Lynch, A. Salvati and K. A. Dawson, *Small*, 2011, **7**, 3341–3349.
14 S. T. Huxtable, D. G. Cahill, S. Shenogin, L. Xue, R. Ozisik, P. Barone, M. Usrey, M. S. Strano, G. Siddons, M. Shim and P. Keblinski, *Nat. Mater.*, 2003, **2**, 731–734.
15 M. S. Dresselhaus, G. Dresselhaus and A. Jorio, *Annu. Rev. Mater. Res.*, 2004, **34**, 247–278.
16 Y. Ding, H. Alias, D. Wen and R. A. Williams, *Int. J. Heat Mass Transfer*, 2006, **49**, 240–250.
17 M. S. Haque, C. Marinelli, F. Udrea and W. I. Milne, 2006 NSTI Nanotechnol. Conf. Trade Show – NSTI Nanotech 2006 Tech. Proc., 2006, 1, 134–137.
18 B. R. Bunes, M. Xu, Y. Zhang, D. E. Gross, A. Saha, D. L. Jacobs, X. Yang, J. S. Moore and L. Zang, *Adv. Mater.*, 2015, **27**, 162–167.
19 B. Latha, P. Kumaresan, S. Nithiyanantham and K. Sampathkumar, *J. Mol. Struct.*, 2018, **1152**, 351–360.
20 S. Mura, J. Nicolas and P. Couvreur, *Nat. Mater.*, 2013, **12**, 991–1003.
21 P. Lemal, C. Geers, C. A. Monnier, F. Crippa, L. Daum, D. A. Urban, B. Rothen-Rutishauser, M. Bonmarin, A. Petri-Fink and T. L. Moore, *J. Magn. Magn. Mater.*, 2017, **427**, 206–211.
22 L. Steinmetz, P. Taladriz-Blanco, C. Geers, M. Spuch-Calvar, M. Bonmarin, S. Balog, B. Rothen-Rutishauser and A. Petri-Fink, *Part. Part. Syst. Charact.*, 2019, **36**, 1900224.
23 O. Breitenstein, W. Warta and M. C. Schubert, *Lock-in Thermography*, Springer International Publishing, 3rd edn, 2018, vol. 10.
24 C. A. Monnier, M. Lattuada, D. Burnand, F. Crippa, J. C. Martinez-Garcia, A. M. Hirt, B. Rothen-Rutishauser, M. Bonmarin and A. Petri-Fink, *Nanoscale*, 2016, **8**, 13321–13332.
25 I. Andreu and E. Natividad, *Int. J. Hyperthermia*, 2013, **29**, 739–751.
26 B. V. Enüstün and J. Turkevich, *J. Am. Chem. Soc.*, 1963, **85**, 3317–3328.
27 K. R. Brown and M. J. Natan, *Langmuir*, 1998, **14**, 726–728.
28 A. Booth and K. A. Jensen, *Protocol for producing reproducible dispersions of manufactured nanomaterials in environmental exposure media*, 2015.
29 A. Hubaux and G. Vos, *Anal. Chem.*, 1970, **42**, 849–855.
30 ATCC, MeT-5A (ATCC ® CRL-9444 ™), https://www.lgcstandards-atcc.org/Products/All/CRL-9444.aspx?geo_country=ch#culturemethod, (accessed 28 April 2020).
31 S. Chortarea, F. Zerimariam, H. Barosova, D. Septiadi, M. J. D. Clift, A. Petri-Fink and B. Rothen-Rutishauser, *Appl. In Vitro Toxicol.*, 2019, **5**, 47–61.
32 S. S. Poulsen, A. T. Saber, A. Williams, O. Andersen, C. Købler, R. Atluri, M. E. Pozzebon, S. P. Mucelli, M. Simion, D. Rickerby, A. Mortensen, P. Jackson, Z. O. Kyjovska, K. Mølhave, N. R. Jacobsen, K. A. Jensen, C. L. Yauk, H. Wallin, S. Halappanavar and U. Vogel, *Toxicol. Appl. Pharmacol.*, 2015, **284**, 16–32.
33 H. H. Gustafson, D. Holt-Casper, D. W. Grainger and H. Ghandehari, *Nano Today*, 2015, **10**, 487–510.
34 D. B. Chithrani and W. C. W. Chan, *Nano Lett.*, 2007, **7**, 1542–1550.
35 N. Oh and J. H. Park, *ACS Nano*, 2014, **8**, 6232–6241.

Open Access Article. Published on 13 August 2020. Downloaded on 2/6/2026 6:09:53 PM.
This article is licensed under a Creative Commons Attribution 3.0 Unported Licence.

36 W. Zhu, A. von dem Bussche, X. Yi, Y. Qiu, Z. Wang, P. Weston, R. H. Hurt, A. B. Kane and H. Gao, *Proc. Natl. Acad. Sci. U. S. A.*, 2016, **113**, 12374–12379.
37 D. Jaque, L. Martínez Maestro, B. del Rosal, P. Haro-Gonzalez, A. Benayas, J. L. Plaza, E. Martín Rodríguez and J. García Solé, *Nanoscale*, 2014, **6**, 9494–9530.
38 H. Chen, L. Shao, T. Ming, Z. Sun, C. Zhao, B. Yang and J. Wang, *Small*, 2010, **6**, 2272–2280.
39 J. Rejman, V. Oberle, I. S. Zuhorn and D. Hoekstra, *Biochem. J.*, 2004, **377**, 159–169.
40 S. E. A. Gratton, P. A. Ropp, P. D. Pohlhaus, J. C. Luft, V. J. Madden, M. E. Napier and J. M. DeSimone, *Proc. Natl. Acad. Sci. U. S. A.*, 2008, **105**, 11613–11618.
41 I. Lynch and K. A. Dawson, *Nano Today*, 2008, **3**, 40–47.
42 E. Casals, T. Pfaller, A. Duschl, G. J. Oostingh and V. Puntes, *ACS Nano*, 2010, **4**, 3623–3632.
43 M. P. Monopoli, D. Walczyk, A. Campbell, G. Elia, I. Lynch, F. Baldelli Bombelli and K. A. Dawson, *J. Am. Chem. Soc.*, 2011, **133**, 2525–2534.
44 T. L. Moore, L. Rodriguez-Lorenzo, V. Hirsch, S. Balog, D. Urban, C. Jud, B. Rothen-Rutishauser, M. Lattuada and A. Petri-Fink, *Chem. Soc. Rev.*, 2015, **44**, 6287–6305.
45 D. Burnand, A. Milosevic, S. Balog, M. Spuch-Calvar, B. Rothen-Rutishauser, J. Dengjel, C. Kinnear, T. L. Moore and A. Petri-Fink, *Small*, 2018, **14**, 1802088.
46 T. L. Moore, D. A. Urban, L. Rodriguez-Lorenzo, A. Milosevic, F. Crippa, M. Spuch-Calvar, S. Balog, B. Rothen-Rutishauser, M. Lattuada and A. Petri-Fink, *Sci. Rep.*, 2019, **9**, 1–9.
47 L. Li, Y. Zhang and J. Wang, *R. Soc. Open Sci.*, 2017, **4**, 170063.
48 H. Gao, W. Shi and L. B. Freund, *Proc. Natl. Acad. Sci. U. S. A.*, 2005, **102**, 9469–9474.
49 C. Kinnear, T. L. Moore, L. Rodriguez-Lorenzo, B. Rothen-Rutishauser and A. Petri-Fink, *Chem. Rev.*, 2017, **117**, 11476–11521.
50 H. Nagai, Y. Okazaki, S. H. Chew, N. Misawa, Y. Yamashita, S. Akatsuka, T. Ishihara, K. Yamashita, Y. Yoshikawa, H. Yasui, L. Jiang, H. Ohara, T. Takahashi, G. Ichihara, K. Kostarelos, Y. Miyata, H. Shinohara and S. Toyokuni, *Proc. Natl. Acad. Sci. U. S. A.*, 2011, **108**, E1330–E1338.
51 D. Septiadi, L. Rodriguez-Lorenzo, S. Balog, M. Spuch-Calvar, G. Spiaggia, P. Taladriz-Blanco, H. Barosova, S. Chortarea, M. J. D. Clift, J. Teeguarden, M. Sharma, A. Petri-Fink and B. Rothen-Rutishauser, *Nanomaterials*, 2019, **9**, 1–13.
52 L. Jianzhong, S. Xing and Y. Zhenjiang, *J. Aerosol Sci.*, 2003, **34**, 909–921.
53 S. R. Price, C. Kinnear and S. Balog, *Nanoscale*, 2019, **11**, 5209–5214.

This journal is © The Royal Society of Chemistry 2020